HHS Public Access

Author manuscript

Acta Biomater. Author manuscript; available in PMC 2017 December 01.

Published in final edited form as:

Acta Biomater. 2016 December ; 46: 221–233. doi:10.1016/j.actbio.2016.09.026.

In vitro and *in vivo* assessment of controlled release and degradation of acoustically-responsive scaffolds

Alexander Moncion[1,2], **Keith J. Arlotta**[2], **Eric G. O'Neill**[2], **Melissa Lin**[2], **Lily A. Mohr**[2], **Renny T. Franceschi**[3,4,5], **Oliver D. Kripfgans**[1,2,3], **Andrew J. Putnam**[3], and **Mario L. Fabiilli**[1,2]

[1]Applied Physics Program, University of Michigan, Ann Arbor, MI USA

[2]Department of Radiology, University of Michigan Health System, Ann Arbor, MI USA

[3]Department of Biomedical Engineering, University of Michigan, Ann Arbor, MI USA

[4]School of Dentistry, University of Michigan, Ann Arbor, MI USA

[5]Department of Biological Chemistry, University of Michigan Medical School, Ann Arbor, MI USA

Abstract

Spatiotemporally controlled release of growth factors (GFs) is critical for regenerative processes such as angiogenesis. A common strategy is to encapsulate the GF within hydrogels, with release being controlled via diffusion and/or gel degradation (i.e., hydrolysis and/or proteolysis). However, simple encapsulation strategies do not provide spatial or temporal control of GF delivery, especially non-invasive, on-demand controlled release post implantation. We previously demonstrated that fibrin hydrogels, which are widely used in tissue engineering and GF delivery applications, can be doped with perfluorocarbon emulsion, thus yielding an acoustically responsive scaffold (ARS) that can be modulated with focused ultrasound, specifically via a mechanism termed acoustic droplet vaporization. This study investigates the impact of ARS and ultrasound properties on controlled release of a surrogate payload (i.e., fluorescently-labeled dextran) and fibrin degradation *in vitro* and *in vivo*. Ultrasound exposure (2.5 MHz, peak rarefactional pressure: 8 MPa, spatial peak time average intensity: 86.4 mW/cm^2), generated up to 7.7 and 21.7-fold increases in dextran release from the ARSs in vitro and in vivo, respectively. Ultrasound also induced morphological changes in the ARS. Surprisingly, up to 2.9-fold greater blood vessel density was observed in ARSs compared to fibrin when implanted subcutaneously, even without delivery of pro-angiogenic GFs. The results demonstrate the potential utility of ARSs in generating controlled release for tissue regeneration.

Graphical abstract

Corresponding Author: Alexander Moncion, M.S, University of Michigan, 3225 Medical Sciences Building I, 1301 Catherine Street, Ann Arbor, MI 48109-5667, Phone: 305-546-6496, ambaez@umich.edu.

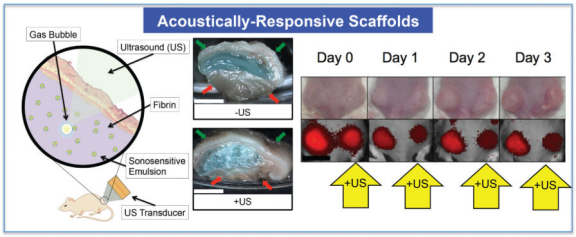

Keywords

acoustic droplet vaporization; ultrasound; spatiotemporal delivery; controlled release; emulsion; perfluorocarbon; fibrin; subcutaneous

1. Introduction

Fibrin hydrogels are biomaterials that are commonly used in tissue engineering as a foundational matrix for tissue fabrication [1-3]. These hydrogels are formed via the enzymatic polymerization of fibrinogen in the presence of thrombin [4] and have many biological advantages versus other hydrogels. Fibrin plays a role in natural wound healing and can be derived from a patient's own blood for the fabrication of autologous hydrogel scaffolds [5]. In addition, being a native protein based biomaterial, enzymatic degradation of fibrin hydrogels occur over time with minimal inflammatory response. The viscoelastic properties of fibrin based implants are relatively low compared to other biomaterials [6], which helps facilitate cellular migration and proliferation into the hydrogel.

Fibrin hydrogels can be seeded with cells and/or other molecular payloads – such as proteins, genes, or drugs - that aid in tissue regeneration [7]. In a conventional fibrin matrix, passive diffusion of the entrapped payload yields a burst release [8]. This limits the ability to sustain release of the payload, unless the payload-scaffold affinity is increased (e.g., modification of fibrin using bioactive peptides [9]) or the payload diffusivity is decreased (e.g., incorporation of heparin [10-12], alteration of crosslinking [13, 14]). Another method of limiting payload diffusivity is by encapsulating the payload into colloidal particles - such as liposomes, polymeric spheres, or emulsions – which are then incorporated into fibrin [15]. However, payload release from these fibrin-colloid composites is still dominated by endogenous processes such as particle and/or scaffold degradation as well as payload diffusion.

During endogenous tissue regeneration, expression of bioactive molecules (e.g., growth factors (GFs)) is regulated both spatially and temporally [16, 17]. This has motivated the development of scaffolds where payload release can be modulated spatiotemporally. Control of payload release has been realized by designing particles that release payload in response to an externally modulated stimulus – such as light, electricity, magnetic fields, temperature – or microenvironmental factors like pH and enzymatic activity [10, 11, 18-24]. These active scaffolds (e.g., hydrogels that contain stimulus-responsive particles) and the means of interacting with them (i.e., modulating stimulus) provide increased control over the biochemical and mechanical microenvironment within the hydrogel. However, clinical

translation of these active scaffolds has been hindered by issues related to biocompatibility, biodegradability, spatiotemporal targeting of the modulating stimulus, or penetration of the stimulus into the body [25, 26].

Ultrasound (US), in conjunction with sonosensitive particles, has been studied as a means of interacting with active scaffolds to achieve both spatial and temporal control exogenously [27, 28]. US can be applied non-invasively, focused with sub-millimeter precision, and reach deeply located implants. US-sensitive hydrogels can be fabricated by doping the scaffold with sonosensitive emulsions or microbubbles, the latter of which are used clinically for contrast enhanced US imaging [27, 29]. Possessing greater stability than microbubbles, sonosensitive emulsions are composed of nano- or micron-sized droplets, contain a liquid perfluorocarbon (PFC) core, and are stabilized by a surfactant shell. PFC emulsions typically contain perfluoropentane (C_5F_{12}, 29°C boiling point) or perfluorohexane (C_6F_{14}, 56°C boiling point) as the dispersed phase and are used because of their biocompatibility and inertness, a general characteristic of PFCs. In addition, sonosensitive emulsions can be formulated as double emulsions such that a payload, like a GF, is encapsulated within their inner aqueous phase [30-32]. Upon exposure to US, the PFC phase within each droplet of the emulsion vaporizes into a gas bubble in a process known as acoustic droplet vaporization (ADV) [33], thus releasing the encapsulated payload to the surrounding environment. Acoustically-responsive scaffolds (ARSs), comprising fibrin scaffolds doped with sonosensitive emulsion, are highly tunable since emulsion (e.g., structure, size), scaffold (e.g., density, geometry), and US properties (e.g., frequency, amplitude) can be easily modified [34]. Compared to approaches using unfocused, low-frequency (i.e., 20 kHz) US [35, 36], the use of focused, high frequency (i.e., > 1 MHz) US to trigger ADV and payload release from an ARS could enable higher spatial resolution, even within deeply-located implants.

We have previously characterized the acoustic mechanisms occurring in ARSs [34]. Additionally, we demonstrated, in a proof-of-concept *in vitro* study with ARSs, that US can control the release of GF (i.e., basic fibroblast growth factor), where bioactivity of the released GF was confirmed using a cellular metabolic assay [27]. This work builds upon these previous publications and focuses on the impact of ARS composition – including varying types of PFCs (i.e., C_5F_{12}, C_6F_{14}, and an ad-mixture) and emulsion size distribution - and US properties (i.e., pressure, US dose, pulse repetition frequency, and time of initial exposure) on the controlled release of a surrogate payload (i.e., dextran) using *in vitro* and *in vivo* models. In addition, this current study investigates the scaffold degradation of the ARSs *in vitro* and *in vivo*, as well as scaffold morphology and vascular in-growth for ARSs.

2. Materials and Methods

2.1 Double Emulsion Preparation and Characterization

Double emulsions with a water-in-PFC-in-water (W_1/PFC/W_2) structure were prepared by modifying a previous method [30]. Briefly, a triblock fluorosurfactant, consisting of Krytox 157FSH (CAS# 51798-33-5, DuPont, Wilmington, DE, USA) and polyethylene glycol (MW: 1000, CAS#: 24991-53-5, Alfa Aeser, Ward Hill, MA USA), was dissolved in 1g of perfluorocarbon (PFC) at 2% (w/w). The PFC phase consisted of perfluoropentane

(subsequently referred to as "C_5", CAS#: 678-26-2, Strem Chemicals, Newburyport, MA USA), perfluorohexane (subsequently referred to as "C_6", CAS#: 355-42-0, Strem Chemicals), or a 1:1 (w/w) C_5:C_6 admixture. The PFC solution was then combined, in a 2:1 volumetric ratio, with an aqueous solution of Alexa Fluor 680-labeled dextran (MW: 10,000 Da, Life Technologies, Grand Island, NY USA) reconstituted at 0.625 mg/mL in Dulbecco's Phosphate-Buffered Saline (DPBS, Life Technologies). This concentration of dextran was chosen to prevent self-quenching of the fluorophore. The phases were sonicated (CL-188, QSonica, LLC, Newton, CT USA) for 30 seconds while on ice. The resulting primary emulsion, with a water-in-PFC (W_1/PFC) structure, was added drop wise to a solution of 50 mg/mL Pluronic F68 (CAS# 9003-11-6, Sigma-Aldrich, St. Louis, MO USA) in DPBS and stirred with a magnetic stir bar at 700 RPM for 2 minutes while on ice. The particle size of the resulting coarse double emulsion (W_1/PFC/W_2) was reduced using a homogenizer (T10, IKA Works Inc., Wilmington, NC USA). Emulsions with "large" and "small" droplet distributions were processed at ~7.9 kRPM and ~29.9 kRPM, respectively. Blank emulsions were prepared as described above with only DPBS as the W_1 phase.

Emulsions were stored at 5°C for 30 minutes and characterized with a Coulter Counter (Multisizer 4, Beckman Coulter, Brea, CA USA) in the range of 1-30 μm. The encapsulation efficiency of the emulsions, defined as the amount of dextran encapsulated in the emulsion divided by the amount of dextran initially loaded into the emulsion, was determined by breaking diluted emulsion in a vacuum oven (23°C, Isotemp Vacuum Oven Model 282A, Pittsburgh, PA USA). The ADV threshold of each emulsion formulation was determined using a previously described method [34]. The structure, composition, and physical parameters of all double emulsion formulations used in this study are listed in Table 1.

2.2 ARS Fabrication

ARSs were prepared using 10 mg/mL clottable protein by first combining bovine fibrinogen (Sigma-Aldrich, 75% total protein, 96% clottable protein) - dissolved in degassed (36% O_2 saturation) Dulbecco's modified Eagle's medium (DMEM, Life Technologies) - with bovine thrombin (20 U/mL, Thrombin-JMI, King Pharmaceuticals, Bristol, TN, USA), 0.025 U/mL aprotinin (Sigma-Aldrich), and 1% (v/v) emulsion. For *in vitro* studies, 0.5 mL aliquots of the ARS mixture were added into each well of a 24 well BioFlex plate (Flexcell International, Burlington, NC, USA) and allowed to polymerize for 30 min at room temperature. Each ARS was then covered with 0.5 mL of overlying media, consisting of DMEM supplemented with 100 U/mL penicillin and 100 μg/mL streptomycin. The ARSs were placed in a humidified incubator at 37°C with 5% carbon dioxide between US exposures.

2.3 US Exposure

All acoustic exposures were conducted using the following setup. A calibrated transducer (2.5 MHz, H108, f-number = 0.83, focal length = 50 mm, Sonic Concepts, Inc., Bothell, WA USA) was driven by pulsed waveforms generated using a dual channel function generator (33500B, Agilent Technologies, Santa Clara, CA USA), amplified by a gated radio frequency amplifier (GA-2500A Ritec Inc, Warwick, RI USA), and passed through a matching circuit (H108_3MN, Sonic Concepts) to reduce impedance between the transducer

and amplifier (Figure 1 (a-I)). Waveform gating was realized using the second channel of the function generator. All generated and amplified signals were monitored with an oscilloscope (HDO4034, Teledyne LeCroy, Chestnut Ridge, NY USA). All acoustic exposures were done with the following parameters unless otherwise stated in the figure caption: 8 MPa peak rarefactional pressure, 13 acoustic cycles, and 100 Hz pulse repetition frequency (PRF). This corresponds to a spatial peak time average intensity of 86.4 mW/cm^2.

2.4 *In vitro* Controlled Release of Dextran

For controlled release experiments, the BioFlex plate containing the ARSs was placed in a tank of degassed water (30-36% O_2 saturation) at 37°C such that only the bottom half of the plate was submerged, as shown in Figure 1 (a). The single element US transducer was positioned under the plate such that the axial focus was located at mid-height of the ARS. The bottom of each well in the plate consisted of a silicone elastomer membrane, which based on a thickness of 1 mm, attenuates the US by less than 2% [37]. During US exposure, the transducer was rastered across the entire ARS for 2 min. Four US exposure conditions were explored: no US, a single US exposure one day after polymerization, a single US exposure four days after polymerization, and daily US for a period of 6 days beginning one day after polymerization. To quantify the amount of dextran released, 50% of the overlying media was collected and replaced with an equal volume of fresh media immediately after every US exposure. The concentration of dextran in the media was measured with a fluorometer (Molecular Devices Spectramax M2e, Sunnyvale, CA USA, 679 nm EX/ 702 nm EM). As a comparison, the release of dextran – incorporated directly in fibrin scaffolds with and without any blank emulsion - was also measured.

2.5 *In vitro* Fibrin Degradation

ARSs were prepared in 24-well BioFlex plates as described previously except with blank C_6 emulsion and Alexa Fluor 647-labeled fibrinogen (Molecular Probes). The final concentration of labeled fibrinogen in each ARS was 0.125 mg/mL; this concentration was chosen to prevent self-quenching of the labeled fibrinogen. The ARSs were exposed to US (as described in Section 2.4) and incubated between US exposures. To quantify the amount of fibrin degradation 50% of the media was collected and replaced with fresh media after every US exposure. The concentration of labeled fibrinogen in the media was measured with a fluorometer (650 nm EX/ 668 nm EM). As a control, fibrin scaffolds without emulsion but with labeled fibrinogen were prepared, and their degradation was quantified similarly.

2.6 *In vivo* Controlled Release of Dextran

This *in vivo* research was conducted with approval of the Institutional Animal Care & Use Committee at the University of Michigan. Female BALB/c mice (n = 22, 18-21 g, Charles River Laboratories, Wilmington, MA, USA) were anesthetized with isoflurane (5% for induction and 1.5% for maintenance). The lower dorsal hair was removed by shaving and depilatory cream (Nair, Church & Dwight Co, Ewing, NJ USA); the skin was sterilized with betadine surgical scrub (Purdue Products L.P., Stamford, CT USA). The ARS mixture (0.25 mL per implant) was then injected subcutaneously using a 20 gauge needle (Becton Dickinson, Franklin Lakes, NJ, USA) at two locations with the dorsal region and allowed to polymerize for 2 minutes prior to removal of the needle. The ARS mixture contained 1%

(v/v) dextran-loaded emulsion with either 1:1 C_5:C_6 or C_6 as the PFC phase. The mice were allowed to recover following implantation. Fibrin scaffolds without emulsion, but containing dextran, were injected as control implants. Blank scaffolds (i.e., without emulsion and dextran) were injected as sham controls.

Figure 1(b) shows the experimental setup used for all *in vivo* studies. Each mouse was anesthetized with isoflurane and placed in a prone position. US coupling gel (MediChoice, Owens & Minor, Mechanicsville, VA USA) was applied to the implant region. A coupling cone (C106, Sonic Concepts) was placed on the US transducer, filled with degassed water (30-36% O_2 saturation), and the water was sealed in by Tegaderm film (3M Health Care, St. Paul, MN USA). The transducer was rastered across the implant for 2 min. For each mouse, US was applied daily to only one scaffold beginning one day after implantation for a period of 10 days. The scaffolds receiving US treatment (i.e., left or right implant) were randomized for all mice.

2.7 *In Vivo* Fibrin Degradation

ARSs containing 1% (v/v) blank emulsion, with C_6 as the PFC phase, and labeled fibrinogen (0.125 mg/mL) were prepared, injected into female BALB/c mice (n = 10), and exposed to US as described in sections 2.5 and 2.6. Fibrin scaffolds without emulsion, but containing labeled fibrinogen, were injected as control implants. Blank scaffolds (i.e., without emulsion and labeled fibrinogen) were injected as sham controls.

2.8 IVIS Imaging

The mice were anesthetized with isoflurane and imaged with an IVIS Spectrum Preclinical In Vivo Imaging System (f/4, field of view = 19.4 cm, Perkin Elmer, Houston, TX USA) at the University of Michigan Center for Molecular Imaging to quantify the fraction of dextran or fibrinogen released from the implants [38]. The mice were imaged on day 0 (i.e., the day of implantation), 1 (i.e., the first day of US exposure), 2, 3, 4, 7, and 10. On days 1-10, the mice were imaged after US exposure. For the dextran release study, the fluorophore signal was collected using an excitation filter of 675 nm and emission filters ranging from 720 to 780 nm. To account for autofluorescence, a sequence of background signals was collected using an excitation filter of 605 nm and emission filters ranging from 660 to 780 nm. For the fibrin degradation study, the fluorophore signal was collected using an excitation filter of 640 nm and emission filters ranging from 680 to 740 nm. To account for autofluorescence, a sequence of background signals was collected using an excitation filter of 570 nm and emission filters ranging from 620 to 740 nm. Spectral unmixing was performed on the dextran and fibrinogen data sets in Living Image software (Perkin Elmer), according to the manufacturer's instructions, using the fluorophore and autofluorescence (background) images. Following unmixing, equally sized regions of interest (ROIs, 1.25 cm diameter) corresponding to each implant, were drawn and the average radiant efficiency ([photons/s/cm^2/sr]/[μW/cm^2]) was calculated. The size of the ROI, f/stop, and field of view were sufficiently large to encompass any lateral and axial diffusion of the dextran after release. For each implant, the average radiant efficiency on days 1-10 was normalized by the day 0 measurement, thus accounting for any differences in the amount of fluorophore initially loaded.

2.9 Histology

For the *in vivo* fibrin degradation study, mice were euthanized on day 3 and day 10 post implantation. ARSs were retrieved and fixed overnight in aqueous buffered zinc formalin (CAS# 50-00-0, Formalde-Fresh, Fisher Scientific). Implants were then transferred to 70% ethanol until they were processed and embedded in paraffin at the University of Michigan Microscopy & Image Analysis Laboratory. The paraffin-embedded tissues were cut into 5 μm thick serial sections and placed on pre-cleaned glass slides (Fisherbrand Superfrost Plus, Fisher Scientific) for histological analysis. Tissue sections were stained with Modified Harris Formulation hematoxylin (Ricca Chemical Company, Arlington, TX USA) and aqueous eosin Y solution (0.25% (w/v) in 57% (v/v) alcohol, Sigma-Aldrich) (H&E) to visualize the overall tissue morphology. Immunostaining of mice-derived blood vessels was performed using a rabbit anti-mouse CD31 primary antibody (ab28364, Abcam, Cambridge, MA USA) combined with a goat anti-rabbit secondary labeled polymer-horseradish peroxidase conjugate (Envision+ System-HRP (DAB), Dako North America, Inc., Carpinteria, CA USA), as described previously [39, 40]. Negative controls, involving staining with a rabbit IgG polyclonal isotype control (ab27478, Abcam) as the primary antibody or staining with the secondary antibody only, confirmed the specificity of the CD31 staining. Tissue sections were visualized and photographed with a Leica DMRB light microscope (Leica Microsystems, Inc., Buffalo Grove, IL USA). Three tissue sections from each implant–with five images per tissue section – were analyzed manually for blood vessel formation per unit area as well as thickness of the granulation layer. Blood vessel counting was done, in a blinded manner, by three separate individuals. Blood vessels were identified in CD31-stained tissues at 20x magnification by defined lumens and complete enclosure of the lumen.

2.10 Statistics

All statistical analyses were performed using GraphPad Prism software (GraphPad Software, Inc., La Jolla, CA USA). All data is expressed as the mean ± standard error of the mean of measured quantities. All *n*-values are listed below each corresponding figure. The 95% confidence intervals of slopes are listed in the format S [S_L, S_H], where S is the average slope, S_L is the lower bound slope, and S_H is the upper bound slope. Statistically significant differences of all other data sets were determined with a Student's *t*-test corrected for multiple comparisons using the Holm-Sidak method, with differences deemed significant for $p<0.05$.

Results

3.1. Emulsion Properties

As listed in Table 1, each "large" emulsion displayed a larger mean droplet diameter and smaller number concentration compared to the "small" emulsion for a given PFC core. A higher ADV threshold was observed for the small C_6 emulsion when compared to the large C_6 emulsion, while the large C_5 emulsion had a higher payload encapsulation efficiency compared to the small C_5 emulsion. The droplet number concentration and ADV threshold correlated with the fraction of C_6 in the PFC core while the mean droplet diameter correlated

inversely. Example droplet distributions, comparing small and large emulsions, are shown in Figure 2(a).

3.2 *In vitro* Controlled Release of Dextran from ARSs

With US applied daily beginning on day 1, Supplemental Figure 1(a,b) shows that the amount of dextran released from a C_5/C_6-ARS with large emulsion correlated with acoustic pressure and PRF. The acoustic condition that yielded the greatest release was 8 MPa and 100 Hz PRF (40.0 ± 0.8% released by day 6). This acoustic condition was used for all subsequent studies. Comparatively, US exposures at 3 MPa and 100 Hz PRF or 8 MPa and 10 Hz PRF yielded 13.2 ± 0.7% and 29.6 ± 0.7% release by day 6, respectively. The negative control (i.e., −US) exhibited 3.8 ± 0.7% payload release by day 6. With US applied daily beginning on day 4, supplemental Figure 1(c) demonstrates that delayed release is also possible.

The release profiles of ARSs with varying emulsion formulations (i.e., C_5-ARS, C_5/C_6-ARS, and C_6-ARS) and emulsion sizes (i.e., large and small) are shown in Supplemental Figure 2(a-b) and Figure 3(a-d). Three acoustic exposures were explored: −US, +US (day 1 only), and +US (daily beginning on day 1). Without US exposure, no statistically significant differences were observed between ARSs with small and large emulsions (for the same PFC type) by day 6. However the release from C_5-ARSs was statistically higher than both C_5/C_6-ARS, and C_6-ARS on day 6 in the absence of US.

In the presence of US, the amount of dextran released correlated inversely with the amount of C_6 in the PFC core of the emulsion and directly with the number of US exposures. With the large emulsion, a single US exposure (i.e., +US on day 1) produced 20.1 ± 1.5% and 12.1 ± 1.5% dextran release for C_5/C_6-ARS and C_6-ARS by day 6, respectively, while daily US exposure yielded 38.6 ± 1.6% and 22.2 ± 1.3% dextran release by day 6, respectively. For the small emulsion, daily US exposure produced 23.0 ± 1.8% and 14.8 ± 0.4% dextran release for C_5/C_6-ARS and C_6-ARS, respectively. For C_5/C_6-ARS and C_6-ARS with large emulsions, both +US conditions were statistically different from −US starting on day 1, while differences between the two +US exposure conditions began on day 2. For the small emulsions, there were significant differences between +US (daily) and −US starting on day 1 for C_5/C_6-ARS and day 2 for C_6-ARS. The greatest release was observed with C_5-ARS with 15.2 ± 1.0% and 23.5 ± 6.3% release by day 6 for small and large emulsions, respectively. Significant differences between each distributions +/−US conditions started on day 1.

3.3 *In vitro* Enhanced Release of Dextran from Fibrin

Figure 4(a) shows that US increased the release of non-encapsulated dextran from a conventional fibrin gel (i.e., without emulsion). Burst release of the dextran was clearly observed on day 1 (i.e., 1 day after polymerization) with 64.0± 1.8, 72.0 ± 0.7, and 72.2 ± 0.5% released for −US, +US (day 1 only), +US (daily), respectively). Thus, exposure to US generates an additional 8.3 ± 0.1% (absolute) release of dextran for both +US conditions relative to −US. By day 6, the maximum amount of dextran released for the three conditions was 88.2 ± 1.2% (−US), 96.6 ± 1.1 (+US day 1 only), and 99.9 ± 0.1 (+US daily). Both +US

conditions were statistically different from the −US case starting on day 1 and were different from each other starting on day 2.

3.4 Effect of US on *In vitro* Fibrin Degradation of Fibrin and ARSs

The rate of fibrin degradation in the ARSs was also measured (Figure 4(b)). By day 6, 44.3 ± 0.8% of the C_6-ARS was degraded for the +US condition while 38.4 ± 0.3% of the C_6-ARS was degraded for the −US condition. Significant differences were observed between +/−US for ARSs starting on day 1. By comparison, for fibrin gels (i.e., without emulsion), 37.0 ± 0.3% and 34.8 ± 0.7% degradation was observed by day 6 for the −US and +US conditions, respectively, with significant differences observed starting on day 2 (data not shown).

3.5 *In vivo* Controlled Release of Dextran and Fibrin Degradation from ARSs

For *in vivo* studies, dextran release from the subcutaneously implanted scaffolds was monitored longitudinally with whole body fluorescence imaging. We hypothesize that upon release of the dextran from the scaffold, the dextran diffused into the local microvasculature and lymphatic vessels [41] and then was ultimately cleared by the systemic circulation. The clearance caused a decrease in fluorescence signal within the ARS, which was quantified via imaging. Figure 5 shows longitudinal photographs and fluorescence images of mice with implanted C_5/C_6- and C_6-ARSs. Over the 10 day study, the ARSs exhibited a slight volumetric expansion, which was more clearly evident for the C_5/C_6-ARSs. Additionally, the fluorescence signal within the ARS exposed to US decreased qualitatively faster than the sham (i.e., −US) ARS, thus indicating greater dextran release from the +US condition.

Using ROIs corresponding to each implant, the fluorescence images were quantified to obtain the *in vivo* release profiles for C_5/C_6-ARS and C_6-ARS (Figure 6(a,b)). Since *in vitro* results demonstrated that daily US exposure yielded greater dextran release than a single US exposure, two acoustic conditions were evaluated *in vivo*: −US and +US (daily beginning on day 1). Figure 6(a) shows that a large fraction of the dextran payload was released from the C_5/C_6-ARSs on day 1 for the +US condition (74.1 ± 2.2%); comparatively, 55.1 ± 1.5%% was released on day 1 for the −US condition. By day 10, the total dextran released was 88.9 ± 0.8% and 65.5 ± 3.3% for +US and −US, respectively. For C_6-ARSs (Figure 6(b)), significant dextran release in response to US was first observed on day 2 (31.1 ± 8.8%), with greater release for +US versus −US occurring between days 3 and 7. Unlike the C_5/C_6-ARSs, a burst release was not observed for −US on day 1. Between days 0 and 3, release from the −US was not statistically different than zero ($p = 0.6$, slope: 2.6 [−17.4, 22.7]). By day 4, non-selective (i.e., −US) payload release started to occur, with −US and +US conditions yielding 33.0 ± 5.4% and 57.9 ± 6.4% released, respectively. By day 10, 51 ± 14.2 and 75.0 ± 6.1% release was observed for the −US and +US conditions, respectively.

The release profile of non-encapsulated dextran, contained within fibrin scaffolds, is displayed in Figure 6(c). Similar to the *in vitro* results with non-encapsulated dextran (Figure 4(a)), significant burst release occurred within the first day after in situ polymerization (76.4 ± 5.4%). This *in vivo* burst release was greater than that observed *in*

vitro for all tested conditions. The total amount of payload released by day 10 was 90.1 ± 3.1%, which was less than that observed *in vitro* for all tested conditions on day 6.

The degradation rate for the implanted fibrin scaffolds, evaluated using fluorescence imaging, is also shown in Figure 6(c). In the absence of US, 66.8 ± 2.3% degradation was observed by day 10. Comparatively, the degradation rate for C_6-ARSs is displayed in Figure 6(d). No differences were observed between −US and +US in terms of degradation rate (p = 0.4, slope of −US: 2.8 [−0.1, 5.7], slope of +US: 3.6 [1.5, 5.8]) or the amount of ARS degraded at any time point. By day 10, the fraction of degradation was 42.8 ± 6.9% and 49.3 ± 5.4% for −US and +US, respectively. Thus, at 10 days after implantation, ARSs were less degraded than fibrin scaffolds of equal fibrin concentration.

3.6 Morphology and Vascularization of Implanted ARSs

H&E images of fibrin and C_6-ARS implants are displayed in Figure 7. All implants appeared similar on day 0, with no cell invasion and implant degradation. Cellular infiltration was observed on days 3 and 10 for both fibrin and ARSs. For ARSs, there was a difference in morphology between the +/−US conditions 3 days after implantation. The +US ARS had large ruptures within the scaffold, presumably caused by droplet vaporization induced by the US exposures beginning on day 1. The morphology of the −US ARS condition began to approach that of the +US ARS condition 10 days after implantation, as is seen with the gas pocket observed in the H&E section (Figure 7, Day 10-II). This finding was consistent with the release observed for the −US condition for C_6-ARS (Figure 6(b)) and the measured fibrin degradation (Figure 6(d)).

As seen in Figure 8, blood vessel in-growth into the fibrin and ARS implants was evaluated immunohistochemically. As expected, no blood vessels were observed in any scaffold on day 0. Blood vessels were observed in the scaffolds beginning on day 3, with a higher density and larger vessels evident by day 10. Blood vessel density (i.e., number of blood vessels per area) within each scaffold is quantified in Figure 9(a). Blood vessel density increased from day 3 (1.3 ± 0.5, 8.4 ± 7.1, and 16.9 ± 8.8 vessels/mm^2) to day 10 (25.5 ± 4.5, 62.1 ± 12.3, and 73.8 ± 7.1 vessels/mm^2) for fibrin, −US ARSs, and +US ARSs, respectively. On day 10, the blood vessel density within an ARS exposed to US was significantly higher than in a fibrin scaffold. Although not statistically significant (p = 0.057), blood vessel density in the −US ARSs was trending higher than in fibrin. The thickness of the granulation layer in each type of implant is quantified in Figure 9(b). The thickness of the granulation layer increased with time, with the greatest thickness observed on day 10 (141.5 ± 7.8, 377.0 ± 29.2, and 376.4 ± 28.7 μm for fibrin, −US ARS, and +US ARS, respectively). Significant differences were observed on day 10 between fibrin and both ARS conditions.

4. Discussion

We have demonstrated how US can be used to modulate the release of a surrogate payload (i.e., dextran) encapsulated within an ARS. Various acoustic parameters have been shown to affect the ADV threshold (i.e., the lowest acoustic pressure at which ADV begins to occur) and efficiency (i.e., the fraction of droplets that vaporize at a given acoustic pressure) of

sonosensitive emulsions and ARSs [34]. For example, ADV thresholds correlate inversely with US pulse duration, insonation frequency, and PRF [33, 34] while ADV efficiency correlates with acoustic pressure [32, 42]. Supplemental Figure 1 and Figure 3 show that payload release – which is directly related to ADV efficiency - correlated with acoustic pressure, PRF, and number of US exposures for both small and large emulsions. In addition, Supplemental Figure 1(c) shows that delayed release of the encapsulated payload is possible. Thus, the temporal control afforded by an ARS could be used to determine the optimum timing (e.g., after inflammation or cell recruitment/proliferation) of growth factor delivery for tissue regeneration or to better elucidate how temporally restricted delivery impacts fundamental regenerative processes [43].

The tunable responsiveness of ARSs is enhanced further when ARS parameters (e.g., matrix stiffness, emulsion surfactant, emulsion size, composition of the PFC core) are modified [34]. We previously demonstrated that the ADV threshold correlated with fibrin density and the bulk boiling point of the PFC core in the emulsion [34] while ADV efficiency correlated inversely with fibrin density for a fixed acoustic amplitude [27]. In this study, the ADV thresholds of the ARSs (Table 1) correlated with the fraction of C_6 in the PFC core and correlated inversely with droplet diameter (for C_6 only). The acoustic pressure used for all release experiments (except Supplemental Figure 1(a)) was 8 MPa, which was significantly higher than the measured ADV thresholds. However complete payload release in response to US was not observed for any of the ARSs, either *in vitro* or *in vivo*, despite complete exposure of the ARSs to US. This is likely a consequence of the polydisperse size distribution of the emulsions used in the ARSs (Figure 2(a)). Since the ADV threshold correlates inversely with droplet diameter [44-46], larger droplets are more likely to undergo ADV, which can decrease the ADV efficiency generated by subsequent US exposures due to the increase in attenuation caused by the formed bubbles. The use of monodispersed emulsions, which have the same ADV threshold [47, 48], and tighter spatial control of US application could increase the maximum release achievable. Additionally, higher PRF (see Supplemental Figure 1(b)) or longer pulse lengths [34] could be used to increase the fraction of payload released following ultrasound exposure.

Overall, the dependence of the ADV threshold and efficiency on the PFC core and droplet size could be used for sequential release of multiple therapeutic payloads. For example, two growth factors could be sequentially delivered from an ARS by encapsulating each growth factor in separate emulsions with varying PFC cores droplet sizes. The first growth factor to be released could be encapsulated in an emulsion with a lower boiling point PFC (or larger droplet size) while the second growth factor could be encapsulated in an emulsion with a higher boiling point PFC (or smaller droplet size). Thus, the first and second growth factors would be released using lower and higher amplitude ultrasound, respectively.

Retention of payload within the ARS (i.e., in the absence of US) is crucial in order to achieve on-demand, controlled release using US. In the absence of US, all ARS formulations displayed significantly better payload retention than non-emulsified dextran contained within fibrin (Figure 4(a), Figure 6(c)). Payload retention in ARSs correlated with the fraction of C_6 in the emulsion for both *in vitro* and *in vivo* results; for a given PFC core, droplet size did not affect payload retention. Although *in vivo* studies with C_5/C_6-ARS

(Figure 6(a)) show a similar release profile to non-encapsulated dextran (Figure 6(c)), ARSs provide the benefit of enhanced blood vessel formation (Figure 9(a)). The emulsification process minimizes the spontaneous vaporization of low boiling point PFCs, like C_5 (29°C bulk boiling point), at homeostatic body temperature (37°C) because of an increase in Laplace pressure, which increases the effective boiling point of the PFC within each droplet [46, 49]. However, C_5-ARSs were not used for *in vivo* studies since they displayed the lowest payload retention in the absence of US (Supplemental Figure 2). This finding was consistent with our previous demonstration that droplet destabilization occurs within a C_5-ARS [34]. It may be possible to further increase payload retention by using a PFC with a higher boiling point or fabricating monodispersed emulsions.

Conversely, payload release in response to US correlated inversely with the fraction of C_6 in the emulsion for both *in vitro* and *in vivo* results. Additionally, greater overall release was observed for large emulsions compared to small. However, the small emulsions yielded ARSs with better homogeneity (Figure 2(b)), and thus were selected for the *in vivo* studies. These differences in payload release are likely related to the effective boiling point of the PFC within the emulsions, which is dependent on both the droplet diameter and bulk PFC boiling point. For example, the bubble point of a 1:1 (w/w) C_5/C_6 ad-mixture is approximately 39 °C, which is in between the boiling points of C_5 or C_6. Thus, recondensation of the gas nucleus formed by ADV within a droplet is more likely as the fraction of C_6 increases, especially if the US pulse duration is short [50, 51], since vaporized C_6 exists as a supercooled gas at 37 °C.

There are some limitations of using dextran as a model payload, especially in the context of developing ARSs for the controlled delivery of growth factors. First, growth factors such as bFGF can display high affinity for fibrin, which can decrease the extent of burst release [52, 53]. Comparatively, as seen in Figure 4(a) and Figure 6(c), significant burst release is observed with dextran in a fibrin scaffold. Second, the bioactivity of growth factors is dependent on the retention of higher levels of protein structure that can be impacted by US [54]. This is not the case with dextran.

The stability of the fibrin matrix is also critical for controlling release from the ARS. Studies have shown that fibrin degradation occurs even in the presence of a protease inhibitor like aprotinin [38, 55], which was used in the preparation of the ARSs. Fibrin degradation was observed *in vitro,* presumably due to protease impurities in the starting fibrinogen material [56], and further enhanced with US (Figure 4(b)). C_6-ARSs displayed better payload retention than C_5/C_6-ARSs both *in vitro* and *in vivo*. However, various factors present *in vivo* that were mitigated or absent *in vitro* could affect payload retention in the ARS. During *in vitro* fibrin degradation, emulsion released from the fibrin matrix of the ARS accumulated at the bottom of each well. During *in vivo* fibrin degradation, however, non-vaporized emulsion released from the fibrin matrix was exposed to the subcutaneous microenvironment. This could lead to emulsion destabilization and non-selective payload release via enzymatic or cellular pathways as well as uptake and clearance by blood and lymphatic vessels [57]. In addition, cellular migration into the ARS could destabilize the emulsion due to the degradation of the fibrin surrounding each droplet, which could alter the interfacial tension between the emulsion and the fibrin. For example, the fraction of dextran

released in the absence of US (i.e., 51 ± 8.2%) for C_6-ARSs at day 10 is similar to the fraction of scaffold degraded (i.e., 42.8 ± 2.6%). With C_5/C_6-ARSs in the absence of US, a burst release was observed *in vivo* on day 1 that was not observed *in vitro*. At this early time point, scaffold degradation is likely not the cause of this burst release. However, the reshaping of the scaffold and forces exerted on the scaffold in the *in vivo* setting (e.g., caused by animal movement) could have caused destabilization of the C_5/C_6-ARSs. Alternatively, the solubilization of the isoflurane anesthetic in the PFC could have also contributed to destabilization [58].

Previous studies demonstrated that non-thermal US can enhance the diffusion of solutes contained within hydrogels, even causing disruption of hydrogel cross-linking [35] or increases in porosity [59]. In this study, US enhanced *in vitro* dextran release, which correlated with an increase in fibrin degradation in fibrin scaffolds (Figure 4). Thus, it is likely that the increase in dextran release was due to changes in the microstructure of the fibrin following US exposure. Changes in fibrin macroporosity were visible *in vivo* in the ARS in response to US at day 3 (Figure 7, Figure 8), though overall ARS degradation by day 10 was less than fibrin scaffolds. Unlike the monotonically increasing degradation observed with fibrin (Figure 6(c)), the rate (i.e., slope) of fibrin degradation for the C_6-ARSs was not statistically different than zero between days 1-7. Previously, we demonstrated that ARS stiffness increases following US exposure [27, 34], which could reduce cellular infiltration and associated fibrin degradation [60, 61]. Additionally, in our previous study, more than 60% viability was observed with cells coencapsuled in an ARS following US exposure at the acoustic parameters used in these experiments (2.5 MHz, 8 MPa, and 13 cycles) [34].

Greater blood vessel formation and granulation layer thickness were observed in ARSs versus fibrin by day 10 (Figure 9), which suggests that vascularization and cell invasion was enhanced by the presence of C_6 emulsion in the fibrin matrix. PFCs are known for having high gas solubility, especially oxygen, with lower boiling point PFCs exhibiting higher oxygen solubilization [62-64]. As such, cells co-encapsulated in hydrogel scaffolds with PFC display higher viability than cells encapsulated without PFC [65, 66]. The PFC within the ARS may be serving as oxygen depots that could attract cells into the ARS. Previous work has shown no statistical difference in blood vessel formation between a conventional fibrin scaffold and a fibrin scaffold loaded with poly(lactic-co-glycolic) acid (PLGA) particles [67]. This suggests that the PFC within the ARS is the likely cause of enhanced angiogenesis. In addition, the presence of emulsion within the ARS may have facilitated cell invasion into the ARS as seen in Figure 9(b). This is demonstrated by H&E images of tissue samples taken on day 3 and 10 (Figure 7), where greater cell invasion is seen in ARSs versus fibrin implants. It is important to note that the granulation layer mentioned in this work is not a fibrous capsule, as fibrous capsules are chronic and impermeable to cells [68]. Additionally, the morphology of the granulation layer observed here is similar to the morphology seen in prior studies [69]. Overall, the finding that ARSs increase vascularization is interesting, given that no growth factors were released in these experiments, and potentially useful in future studies involving angiogenesis.

Conclusions

In this study, we demonstrated controlled release of encapsulated dextran from fibrin-based scaffolds using focused, 2.5 MHz US. The release profiles were dependent on ARS (e.g., emulsion size, PFC core) and US (e.g., amplitude, PRF, number of exposures) parameters. Payload retention in the absence of US and payload release due to US correlated directly and inversely with the fraction of C_6 in the ARS. US also increased the release of non-encapsulated dextran from fibrin, which was linked to increased fibrin degradation. Within ARSs, US induced morphological changes associated with the formation of gas bubbles produced by ADV. Greater (i.e., up to 2.9-fold) blood vessel formation occurred in ARSs compared to fibrin scaffolds. Overall, ARSs provide a biocompatible, minimally invasive approach for on-demand, controlled payload release using US, and have potential for use in tissue engineering applications.

Supplementary Material

Refer to Web version on PubMed Central for supplementary material.

Acknowledgements

This work was supported by NIH grant R21AR065010 (MLF) and the Basic Radiological Sciences Innovative Research Award (MLF). AM was supported by the National Science Foundation Graduate Student Research Fellowship (Grant No. DGE 1256260). EGO and ML were supported by funds from the Undergraduate Research Opportunity Program.

References

[1]. Shaikh FM, Callanan A, Kavanagh EG, Burke PE, Grace PA, McGloughlin TM. Fibrin: A natural biodegradable scaffold in vascular tissue engineering. Cells Tissues Organs. 2008; 188(4):333–46. PubMed PMID: ISI:000259725900001. English. [PubMed: 18552484]

[2]. Dehghani F, Annabi N. Engineering porous scaffolds using gas-based techniques. Current Opinion in Biotechnology. Oct; 2011 22(5):661–6. PubMed PMID: ISI:000296114600009. English. [PubMed: 21546240]

[3]. Seliktar D. Designing Cell-Compatible Hydrogels for Biomedical Applications. Science. Jun 1; 2012 336(6085):1124–8. PubMed PMID: ISI:000304647900039. English. [PubMed: 22654050]

[4]. Perka C, Spitzer RS, Lindenhayn K, Sittinger M, Schultz O. Matrix-mixed culture: New methodology for chondrocyte culture and preparation of cartilage transplants. Journal of Biomedical Materials Research. Mar 5; 2000 49(3):305–11. PubMed PMID: WOS:000084323600002. [PubMed: 10602062]

[5]. Lee KY, Mooney DJ. Hydrogels for tissue engineering. Chemical Reviews. Jul; 2001 101(7):1869–79. PubMed PMID: WOS:000170045000001. [PubMed: 11710233]

[6]. Markert CD, Guo X, Skardal A, Bharadwaj S, Zhang Y, Bonin K, Guthold M. How Stiff Is It? Characterizing the micro-scale elastic modulus of hydrogels for use in regenerative medicine. Faseb Journal. Apr.2013 27 PubMed PMID: WOS:000319860505585.

[7]. Rioja AY, Annamalai RT, Paris S, Putnam AJ, Stegemann JP. Endothelial sprouting and network formation in collagen- and fibrin-based modular microbeads. Acta Biomaterialia. Jan.2016 29:33–41. PubMed PMID: WOS:000367490000004. [PubMed: 26481042]

[8]. Ehrbar M, Metters A, Zammaretti P, Hubbell JA, Zisch AH. Endothelial cell proliferation and progenitor maturation by fibrin-bound VEGF variants with differential susceptibilities to local cellular activity. Journal of Controlled Release. Jan; 2005 101(1-3):93–109. PubMed PMID: WOS:000226086800010. [PubMed: 15588897]

[9]. Schense JC, Bloch J, Aebischer P, Hubbell JA. Enzymatic incorporation of bioactive peptides into fibrin matrices enhances neurite extension. Nature Biotechnology. Apr; 2000 18(4):415–9. PubMed PMID: WOS:000086444300024.

[10]. Sakiyama-Elbert SE, Hubbell JA. Development of fibrin derivatives for controlled release of heparin-binding growth factors. Journal of Controlled Release. Apr 3; 2000 65(3):389–402. PubMed PMID: WOS:000085905600006. [PubMed: 10699297]

[11]. Sakiyama-Elbert SE, Hubbell JA. Controlled release of nerve growth factor from a heparin-containing fibrin-based cell ingrowth matrix. Journal of Controlled Release. Oct 3; 2000 69(1): 149–58. PubMed PMID: WOS:000090006800011. [PubMed: 11018553]

[12]. Sakiyama-Elbert SE, Panitch A, Hubbell JA. Development of growth factor fusion proteins for cell-triggered drug delivery. Faseb Journal. May; 2001 15(7):1300–2. PubMed PMID: WOS: 000168655200042. [PubMed: 11344120]

[13]. Jeong B, Bae YH, Lee DS, Kim SW. Biodegradable block copolymers as injectable drug-delivery systems. Nature. Aug; 1997 388(6645):860–2. PubMed PMID: WOS:A1997XT75400044. [PubMed: 9278046]

[14]. Bryant SJ, Anseth KS. The effects of scaffold thickness on tissue engineered cartilage in photocrosslinked poly(ethylene oxide) hydrogels. Biomaterials. Mar; 2001 22(6):619–26. PubMed PMID: WOS:000166842000014. [PubMed: 11219727]

[15]. Fabiilli ML, Haworth KJ, Sebastian IE, Kripfgans OD, Carson PL, Fowlkes JB. Delivery of chlorambucil using an acoustically-triggered perfluoropentane emulsion. Ultrasound in Medicine and Biology. Aug; 2010 36(8):1364–75. PubMed PMID: 20691925. Pubmed Central PMCID: 2933659. Epub 2010/08/10. eng. [PubMed: 20691925]

[16]. Carmeliet P. Angiogenesis in life, disease and medicine. Nature. Dec 15; 2005 438(7070):932–6. PubMed PMID: ISI:000233934600051. English. [PubMed: 16355210]

[17]. Risau W. Mechanisms of angiogenesis. Nature. Apr 17; 1997 386(6626):671–4. PubMed PMID: ISI:A1997WU38700044. English. [PubMed: 9109485]

[18]. Matsusaki M, Akashi M. Novel functional biodegradable polymer IV: pH-Sensitive controlled release of fibroblast growth factor-2 from a poly(gamma-glutamic acid)-sulfonate matrix for tissue engineering. Biomacromolecules. Nov-Dec;2005 6(6):3351–6. PubMed PMID: ISI: 000233392100062. English. [PubMed: 16283765]

[19]. Thornton PD, McConnell G, Ulijn RV. Enzyme responsive polymer hydrogel beads. Chemical Communications. 2005; (47):5913–5. PubMed PMID: ISI:000233775600022. English. [PubMed: 16317473]

[20]. Frimpong RA, Fraser S, Hilt JZ. Synthesis and temperature response analysis of magnetic-hydrogel nanocomposites. Journal of Biomedical Materials Research Part A. 2007; 80A(1):1–6.

[21]. Zhao X, Kim J, Cezar CA, Huebsch N, Lee K, Bouhadir K, Mooney DJ. Active scaffolds for on-demand drug and cell delivery. Proceedings of the National Academy of Sciences of the United States of America. 2011; 108(1):67–72. [PubMed: 21149682]

[22]. Kulkarni R, Biswanath S. Electrically responsive smart hydrogels in drug delivery: a review. Journal of Applied Biomaterials and Biomechanics. 2007; 5(3):125–39. [PubMed: 20799182]

[23]. Wu C, Chen C, Lai J, Mu X, Zheng J, Zhao Y. Molecule-scale controlled-release system based on light-responsive silica nanoparticles. Chemical Communications. 2008; 23:2662–4.

[24]. Lavigne MD, Pennadam SS, Ellis J, Yates LL, Alexander C, Gorecki DC. Enhanced gene expression through temperature profile-induced variations in molecular architecture of thermoresponsive polymer vectors. The Journal of Gene Medicine. 2007; 9(1):44–54. [PubMed: 17167816]

[25]. Qiu Y, Park K. Environment-sensitive hydrogels for drug delivery. Advanced Drug Delivery Reviews. Dec 31; 2001 53(3):321–39. PubMed PMID: WOS:000173232500007. [PubMed: 11744175]

[26]. Bromberg LE, Ron ES. Temperature-responsive gels and thermogelling polymer matrices for protein and peptide delivery. Advanced Drug Delivery Reviews. May; 1998 31(3):197–221. PubMed PMID: WOS:000073418500003. [PubMed: 10837626]

[27]. Fabiilli ML, Wilson CG, Padilla F, Martin-Saavedra FM, Fowlkes JB, Franceschi RT. Acoustic droplet-hydrogel composites for spatial and temporal control of growth factor delivery and

scaffold stiffness. Acta Biomaterialia. Mar 25.2013 PubMed PMID: 23535233. Epub 2013/03/29. Eng.

[28]. Kripfgans OD, Zhang M, Fabiilli ML, Carson PL, Padilla F, Swanson SD, Mougenot C, Fowlkes JB, Mougenot C. Acceleration of ultrasound thermal therapy by patterned acoustic droplet vaporization. J Acoust Soc Am. Jan; 2014 135(1):537–44. PubMed PMID: 24437794. Pubmed Central PMCID: 3985868. [PubMed: 24437794]

[29]. Epstein-Barash H, Orbey G, Polat BE, Ewoldt RH, Feshitan J, Langer R, Borden MA, Kohane DS. A microcomposite hydrogel for repeated on-demand ultrasound-triggered drug delivery. Biomaterials. Jul; 2010 31(19):5208–17. PubMed PMID: ISI:000278466100019. English. [PubMed: 20347484]

[30]. Fabiilli ML, Lee JA, Kripfgans OD, Carson PL, Fowlkes JB. Delivery of water-soluble drugs using acoustically triggered perfluorocarbon double emulsions. Pharm Res. Dec; 2010 27(12): 2753–65. PubMed PMID: 20872050. Pubmed Central PMCID: 3085450. Epub 2010/09/28. eng. [PubMed: 20872050]

[31]. Couture O, Urban A, Bretagne A, Martinez L, Tanter M, Tabeling P. In vivo targeted delivery of large payloads with an ultrasound clinical scanner. Medical Physics. Aug; 2012 39(8):5229–37. PubMed PMID: ISI:000307917600060. English. [PubMed: 22894447]

[32]. Couture O, Faivre M, Pannacci N, Babataheri A, Servois V, Tabeling P, Tanter M. Ultrasound internal tattooing. Medical Physics. Feb; 2011 38(2):1116–23. PubMed PMID: ISI: 000286945000058. English. [PubMed: 21452748]

[33]. Kripfgans, OD. Acoustic droplet vaporization for diagnostic and therapeutic applications. University of Michigan; Ann Arbor, MI: 2002.

[34]. Moncion A, Arlotta KJ, Kripfgans OD, Fowlkes JB, Carson PL, Putnam AJ, Franceschi RT, Fabiilli ML. Design and Characterization of Fibrin-Based Acoustically Responsive Scaffolds for Tissue Engineering Applications. Ultrasound in Medicine and Biology. 2016; 42(1):257–71. [PubMed: 26526782]

[35]. Huebsch N, Kearney CJ, Zhao XH, Kim J, Cezar CA, Suo ZG, Mooney DJ. Ultrasound-triggered disruption and self-healing of reversibly cross-linked hydrogels for drug delivery and enhanced chemotherapy. Proceedings of the National Academy of Sciences of the United States of America. Jul; 2014 111(27):9762–7. PubMed PMID: WOS:000338514800026. [PubMed: 24961369]

[36]. Kennedy S, Hu J, Kearney C, Skaat H, Gu L, Gentili M, Vandenburgh H, Mooney D. Sequential release of nanoparticle payloads from ultrasonically burstable capsules. Biomaterials. Jan.2016 75:91–101. PubMed PMID: WOS:000365373200009. [PubMed: 26496382]

[37]. Garvin KA, Hocking DC, Dalecki D. Controlling the Spatial Organization of Cells and Extracellular Matrix Proteins in Engineered Tissues Using Ultrasound Standing Wave Fields. Ultrasound in Medicine and Biology. Nov; 2010 36(11):1919–32. PubMed PMID: ISI: 000283267200017. English. [PubMed: 20870341]

[38]. Wolbank S, Pichler V, Ferguson JC, Meinl A, van Griensven M, Goppelt A, Redl H. Non-invasive in vivo tracking of fibrin degradation by fluorescence imaging. Journal of Tissue Engineering and Regenerative Medicine. Aug; 2015 9(8):973–6. PubMed PMID: WOS: 000359297700009. [PubMed: 25044309]

[39]. Nor JE, Peters MC, Christensen JB, Sutorik MM, Linn S, Khan MK, Addison CL, Mooney DJ, Polverini PJ. Engineering and characterization of functional human microvessels in immunodeficient mice. Laboratory Investigation. Apr; 2001 81(4):453–63. PubMed PMID: WOS:000168174000003. [PubMed: 11304564]

[40]. Vigen M, Ceccarelli J, Putnam AJ. Protease-Sensitive PEG Hydrogels Regulate Vascularization In Vitro and In Vivo. Macromolecular Bioscience. Oct; 2014 14(10):1368–79. PubMed PMID: WOS:000343872600002. [PubMed: 24943402]

[41]. Richter WF, Bhansali SG, Morris ME. Mechanistic Determinants of Biotherapeutics Absorption Following SC Administration. Aaps Journal. Sep; 2012 14(3):559–70. PubMed PMID: WOS: 000305519900023. [PubMed: 22619041]

[42]. J. BA, B.M. M, M. A, J.D. C, O.N. EG, W. CG, F. RT, F. ML. In Situ Transfection by Controlled Release of Lipoplexes using Acoustic Droplet Vaporization. Advanced Healthcare Materials. 2016; (In Press). doi: 10.1002/adhm.201600008

[43]. Briquez PS, Clegg LE, Martino MM, Mac Gabhann F, Hubbell JA. Design principles for therapeutic angiogenic materials. Nature Reviews Materials. Jan.2016 1(1) PubMed PMID: WOS:000377667000005.

[44]. Fabiilli ML, Haworth KJ, Fakhri NH, Kripfgans OD, Carson PL, Fowlkes JB. The role of inertial cavitation in acoustic droplet vaporization. IEEE Trans Ultrason Ferroelectr Freq Control. May; 2009 56(5):1006–17. PubMed PMID: 19473917. Pubmed Central PMCID: 3085427. Epub 2009/05/29. eng. [PubMed: 19473917]

[45]. Schad KC, Hynynen K. In vitro characterization of perfluorocarbon droplets for focused ultrasound therapy. Physics in Medicine and Biology. Sep; 2010 55(17):4933–47. [PubMed: 20693614]

[46]. Sheeran PS, Wong VP, Luois S, McFarland RJ, Ross WD, Feingold S, Matsunaga TO, Dayton PA. Decafluorobutane as a Phase-Change Contrast Agent for Low-Energy Extravascular Ultrasonic Imaging. Ultrasound in Medicine and Biology. Sep; 2011 37(9):1518–30. PubMed PMID: ISI:000293449400018. English. [PubMed: 21775049]

[47]. Bardin D, Martz TD, Sheeran PS, Shih R, Dayton PA, Lee AP. High-speed, clinical-scale microfluidic generation of stable phase-change droplets for gas embolotherapy. Lab on a Chip. 2011; 11(23):3990–8. 2011. PubMed PMID: WOS:000296737100008. [PubMed: 22011845]

[48]. Martz TD, Sheeran PS, Bardin D, Lee AP, Dayton PA. Precision Manufacture of Phase-Change Perfluorocarbon Droplets Using Microfluidics. Ultrasound in Medicine and Biology. Nov; 2011 37(11):1952–7. PubMed PMID: ISI:000296569700022. English. [PubMed: 21963036]

[49]. Rapoport NY, Kennedy AM, Shea JE, Scaife CL, Nam K-H. Controlled and targeted tumor chemotherapy by ultrasound-activated nanoemulsions/microbubbles. Journal of Controlled Release. 2009; 138(2):268–76. Pubmed Central PMCID: PMC2746980. [PubMed: 19477208]

[50]. Reznik N, Shpak O, Gelderblom EC, Williams R, de Jong N, Versluis M, Burns PN. The efficiency and stability of bubble formation by acoustic vaporization of submicron perfluorocarbon droplets. Ultrasonics. Sep; 2013 53(7):1368–76. PubMed PMID: WOS: 000320598800020. [PubMed: 23652262]

[51]. Rapoport N, Nam KH, Gupta R, Gao ZG, Mohan P, Payne A, Todd N, Liu X, Kim T, Shea J, Scaife C, Parker DL, Jeong EK, Kennedy AM. Ultrasound-mediated tumor imaging and nanotherapy using drug loaded, block copolymer stabilized perfluorocarbon nanoemulsions. Journal of Controlled Release. Jul 15; 2011 153(1):4–15. PubMed PMID: ISI:000293433500002. English. [PubMed: 21277919]

[52]. Yang XC, Wang HJ. Electrospun Functional Nanofibrous Scaffolds for Tissue Engineering. Tissue Engineering. 2010:159–77. PubMed PMID: WOS:000363689000009. [PubMed: 19698058]

[53]. Jeon O, Ryu SH, Chung JH, Kim BS. Control of basic fibroblast growth factor release from fibrin gel with heparin and concentrations of fibrinogen and thrombin. Journal of Controlled Release. Jul; 2005 105(3):249–59. PubMed PMID: WOS:000230807600006. [PubMed: 16088988]

[54]. Marchioni C, Riccardi E, Spinelli S, dell'Unto F, Grimaldi P, Bedini A, Giliberti C, Giuliani L, Palomba R, Castellano AC. Structural changes induced in proteins by therapeutic ultrasounds. Ultrasonics. 2009; 49(6-7):569–76. [PubMed: 19278707]

[55]. Smith JD, Chen A, Ernst LA, Waggoner AS, Campbell PG. Immobilization of aprotinin to fibrinogen as a novel method for controlling degradation of fibrin gels. Bioconjugate Chemistry. May-Jun;2007 18(3):695–701. PubMed PMID: WOS:000246485500013. [PubMed: 17432824]

[56]. Lucas MA, Fretto LJ, McKee PA. The inding of human-plasminogen to fibrin and fibrinogen. Journal of Biological Chemistry. 1983; 258(7):4249–56. PubMed PMID: WOS:A1983QJ80800037. [PubMed: 6833255]

[57]. Ikomi F, Hanna GK, Schmid-Schonbein GW. Size- and surface-dependent uptake of colloid particles into the lymphatic system. Lymphology. Sep; 1999 32(3):90–102. PubMed PMID: WOS:000082525400003. [PubMed: 10494521]

[58]. Cuignet OY, Baele PM, Van Obbergh LJ. A second-generation blood substitute (perflubron emulsion) increases the blood solubility of modern volatile anesthetics in vitro. Anesthesia and Analgesia. Aug; 2002 95(2):368–72. PubMed PMID: WOS:000176964200023. [PubMed: 12145053]

[59]. Guo GP, Lu L, Ji HF, Ma Y, Dong R, Tu J, Guo XS, Qiu YY, Wu JR, Zhang D. Low intensity pulse ultrasound stimulate chondrocytes growth in a 3-D alginate scaffold through improved porosity and permeability. Ultrasonics. Apr.2015 58:43–52. PubMed PMID: WOS: 000349365400007. [PubMed: 25543661]

[60]. Ghajar CM, Chen X, Harris JW, Suresh V, Hughes CCW, Jeon NL, Putnam AJ, George SC. The effect of matrix density on the regulation of 3-D capillary morphogenesis. Biophysical Journal. Mar 1; 2008 94(5):1930–41. PubMed PMID: ISI:000253313800043. English. [PubMed: 17993494]

[61]. Kniazeva E, Putnam AJ. Endothelial cell traction and ECM density influence both capillary morphogenesis and maintenance in 3-D. American Journal of Physiology-Cell Physiology. Jul; 2009 297(1):C179–C87. PubMed PMID: WOS:000268497000020. [PubMed: 19439531]

[62]. Johnson JLH, Dolezal MC, Kerschen A, Matsunaga TO, Unger EC. In vitro comparison of dodecafluoropentane (DDFP), perfluorodecalin (PFD), and perfluoroctylbromide (PFOB) in the facilitation of oxygen exchange. Artificial cells, blood substitutes, and biotechnology. 2009; 37(4):156–62.

[63]. Riess JG. Oxygen Carriers ("Blood Substitutes") - Raison d'Etre, Chemistry, and Some Physiology. Chemical Reviews. 2001; 101(9):2797–919. [PubMed: 11749396]

[64]. Dias AMA, Freire M, Coutinho JAP, Marrucho IM. Solubility of oxygen in liquid perfluorocarbons. Fluid Phase Equilibria. Aug 15.2004 222:325–30. PubMed PMID: WOS: 000223777100041.

[65]. Chin K, Khattak SF, Bhatia SR, Roberts SC. Hydrogel-perfluorocarbon composite scaffold promotes oxygen transport to immobilized cells. Biotechnology Progress. 2008; 24(2):358–66. [PubMed: 18293995]

[66]. Maillard E, Juszczak MT, Clark A, Hughes SJ, Gray DRW, Johnson PRV. Perfluorodecalin-enriched fibrin matrix for human islet culture. Biomaterials. Dec; 2011 32(35):9282–9. PubMed PMID: ISI:000296684200014. English. [PubMed: 21899883]

[67]. Chung YI, Kim SK, Lee YK, Park SJ, Cho KO, Yuk SH, Tae G, Kim YH. Efficient revascularization by VEGF administration via heparin-functionalized nanoparticle-fibrin complex. Journal of Controlled Release. May 10; 2010 143(3):282–9. PubMed PMID: WOS: 000278240300002. English. [PubMed: 20093158]

[68]. Thomson KS, Dupras SK, Murry CE, Scatena M, Regnier M. Proangiogenic microtemplated fibrin scaffolds containing aprotinin promote improved wound healing responses. Angiogenesis. Jan; 2014 17(1):195–205. PubMed PMID: WOS:000329228000015. [PubMed: 24127199]

[69]. Shea LD, Smiley E, Bonadio J, Mooney DJ. DNA delivery from polymer matrices for tissue engineering. Nature Biotechnology. Jun; 1999 17(6):551–4. PubMed PMID: WOS: 000080716500025.

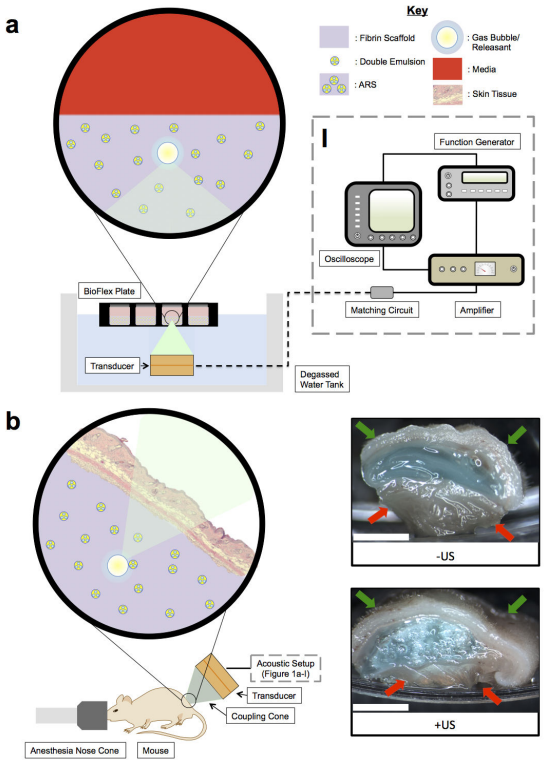

Figure 1.

(a) *In vitro* and (b) *in vivo* setups for US exposure. The equipment used to drive the transducer is depicted in (a-I). (b) Right: Macroscopic images of ARSs containing blank C_6 emulsion and AF647-labeled fibrinogen (blue). The ARSs were harvested 3 days after subcutaneous implantation. Gas bubbles, produced when the US vaporizes the emulsion within the ARS, is evident for the +US condition. The skin surface and underlying muscle are indicated by the green and red arrows, respectively. Scale bar = 0.5 cm.

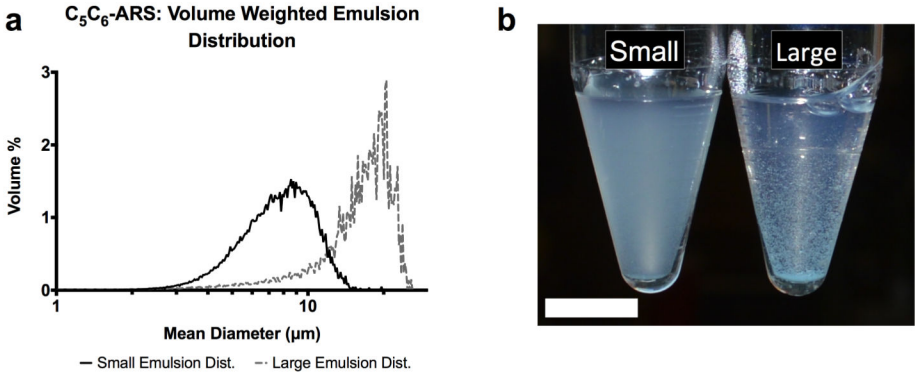

Figure 2.

(a) The volume weighted size distributions of two C_6 emulsion populations – small and large. The different size distributions were obtained by varying the rotational speed of the homogenizer following the second emulsification step. (b) Image of C_6-ARSs with small (left) and large (right) emulsions 1 minute after polymerization. The small emulsion is evenly dispersed in the ARS while some settling is observed for the large emulsion. Scale bar = 1 cm.

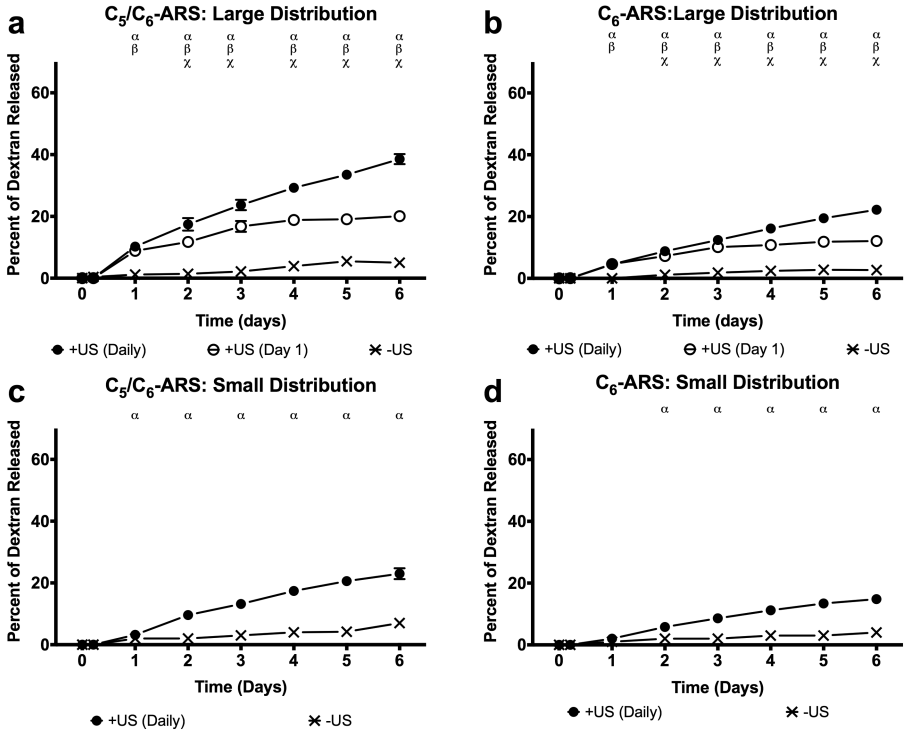

Figure 3.

In vitro release profiles for (a) C_5/C_6-ARSs and (b) C_6-ARSs with large emulsions as well as (c) C_5/C_6-ARSs and (d) C_6-ARSs with a small emulsions. All ARSs contained emulsified dextran and were exposed to one of the following acoustic conditions: −US, +US (day 1 only), and +US (daily beginning on day 1). For all experimental conditions, US exposure was done with the same setup/parameters described in Section 2.3. All data is represented as mean ± standard error of the mean for n = 5 scaffolds. Statistically significant differences ($p < 0.05$) are denoted as follows. α: +US (daily) vs. −US; β: +US (day 1) vs. −US; χ: +US (daily) vs. +US (day 1).

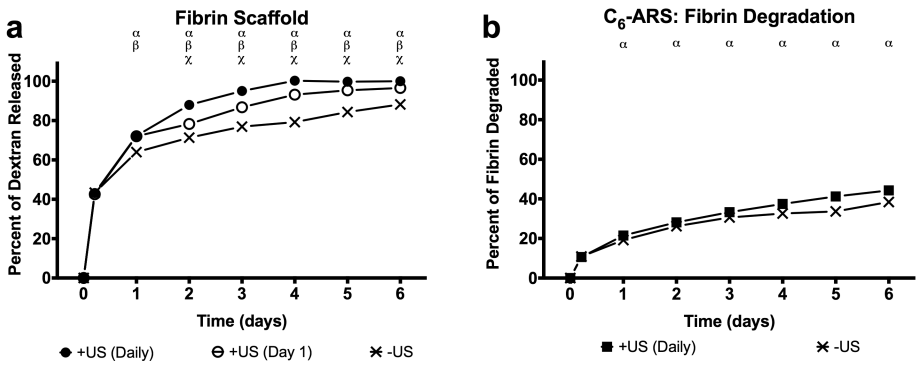

Figure 4.

(a) *In vitro* release profiles of non-encapsulated dextran in a fibrin scaffold exposed to one of the following acoustic conditions: −US, +US (day 1 only), and +US (daily beginning on day 1). (b) Fibrin degradation of ARSs with and without US (daily beginning on day 1). For all experimental conditions, US exposure was done with the same setup/parameters described in Section 2.3. All data is represented as mean ± standard error of the mean for n = 5 scaffolds. Statistically significant differences ($p < 0.05$) are denoted as follows. α: +US (daily) vs. −US; β: +US (day 1) vs. −US; χ: +US (daily) vs. +US (day 1).

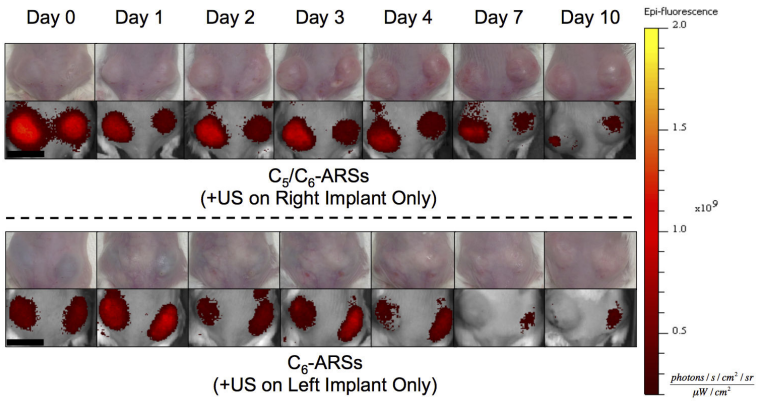

Figure 5.

Longitudinal images, visible and fluorescence, of two mice – each with two subcutaneously implanted ARSs (top: C_5/C_6-ARSs, bottom: C_6-ARSs). The ARSs were implanted on day 0 and US applied daily starting on day 1 to the right (C_5/C_6-ARSs) or left (C_6-ARSs) implant. The colormap is quantitatively indicative of the dextran concentration remaining in the ARS. Scale bar = 1 cm.

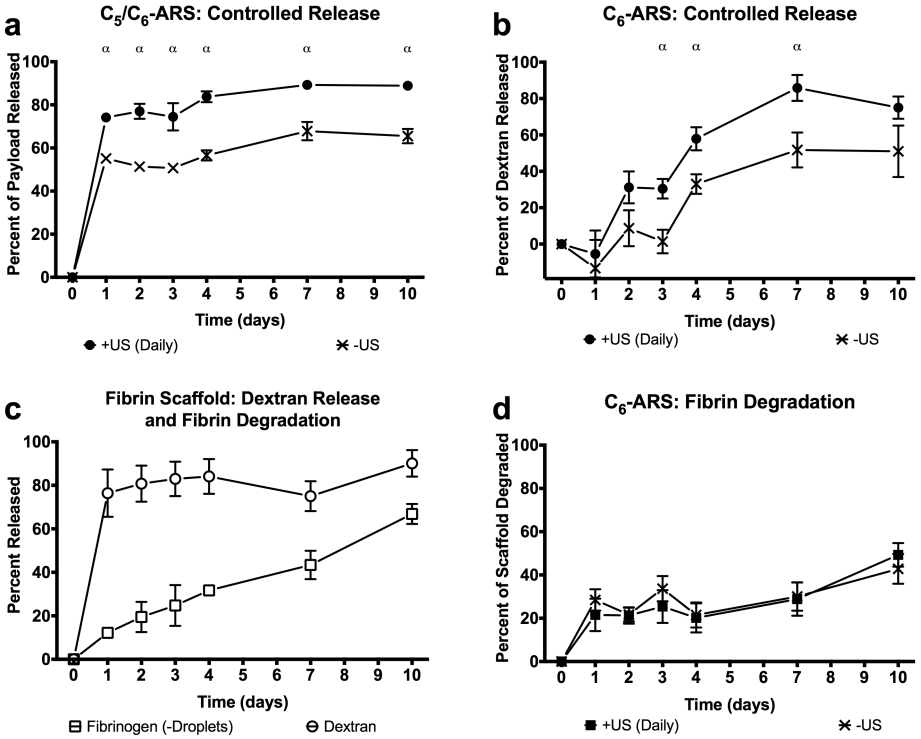

Figure 6.

In vivo release profiles of dextran from (a) C_5/C_6-ARSs with a small emulsion, (b) C_6-ARSs with a small emulsion, or (c) fibrin scaffolds. The scaffolds contained emulsified (a,b) or non-emulsified (c) dextran. *In vivo* fibrin degradation of (c) fibrin and (d) ARSs with blank C_6 emulsion. ARSs were exposed to +US (daily beginning on day 1) or −US using the same setup/parameters described in Section 2.3. All ARSs had a fibrin concentration of 10 mg/mL, were implanted one day prior to the first acoustic exposure, and had a volume of 0.25 mL. All data is represented as mean ± standard error of the mean for n = 11 (a,,b), n = 4 (c), and n = 10 (d) implants/condition. Statistically significant differences ($p < 0.05$) are denoted as follows. α: +US (daily) vs. −US.

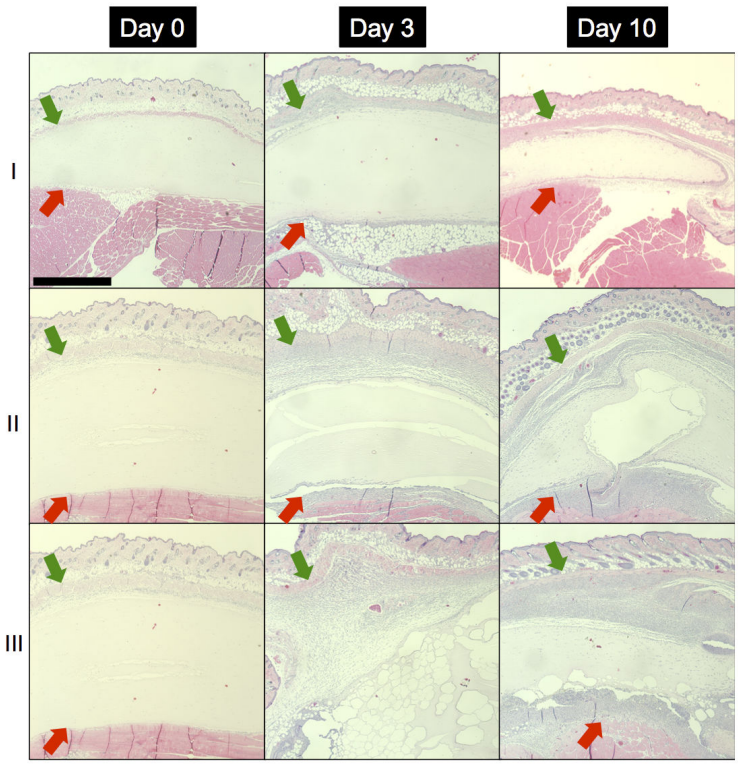

Figure 7.

H&E images of implanted (I) fibrin scaffolds, (II) ARS not exposed to US (i.e., −US), and (III) ARS exposed to daily US beginning on day 1 (i.e., +US) on days 0, 3, and 10 at 5x magnification. The +/−US images of the ARSs are from contralateral implants within the same mouse. The green and red arrows denote the skin/implant interface and implant/(adipose or muscle) interface, respectively. Scale bar = 1 mm.

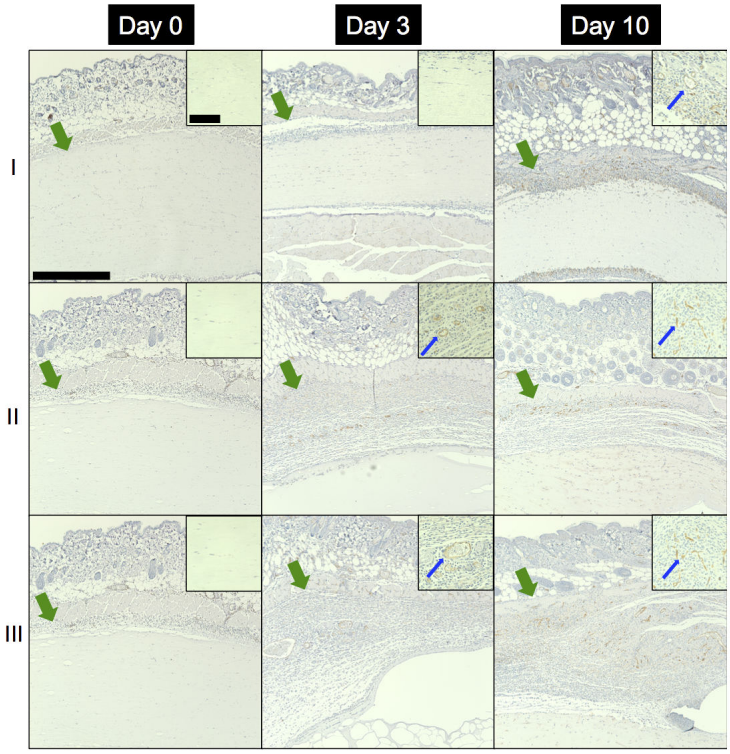

Figure 8.

CD31, with hematoxylin counterstain, images of implanted (I) fibrin scaffolds, (II) C_6-ARSs not exposed to US (i.e., −US), and (III) C_6-ARSs exposed to daily US (beginning on day 1 (i.e., +US)) on days 0, 3, and 10 at 10x magnification. The +/−US images of the ARSs are from contralateral implants within the same mouse. Inset images (63x magnification) are zoomed in within the implant to highlight blood vessel invasion, or lack thereof. The green arrows denote the skin/implant interface while the blue arrows denote blood vessels. Large scale bar = 0.5 mm and the small scale bar = 0.1 mm.

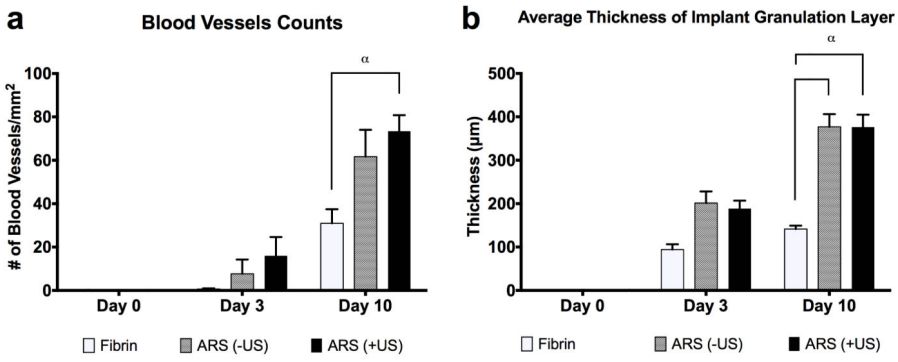

Figure 9.

Quantification of (a) blood vessel density from CD31-stained images and (b) granulation layer thickness from H&E stained images of fibrin scaffolds, C_6-ARSs not exposed to US (i.e., −US), and C_6-ARSs exposed to daily US beginning on day 1 (i.e., +US). All data is represented as mean ± standard error of the mean for n=9. α denotes statistically significant differences ($p < 0.05$).

Table 1

Physical parameters of emulsions used to dope the acoustically responsive scaffolds

			Number Weighted Mean Diameter (μm)		Volume Weighted Mean Diameter (μm)		Droplet Concentration (Number/mL)		ADV Threshold (MPa)		Encapsulation Efficiency (%)	
Perfluorocarbon	**Distribution Size**	**Payload**	**Mean**	**SEM**	**Mean**	**SEM**	**Mean**	**SEM**	**Mean**	**SEM**	**Mean**	**SEM**
100% Perfluoropentane (C_5)	Large	AF680 Dextran	3.5	0.1	21.2	0.5	1.0E + 10	2.2E + 8	1.7	0.2	82.5	7.8
	Small	AF680 Dextran	3.0	0.1	11.8	0.2	7.4E + 10	8.2E + 8	1.9	0.1	50.1	9.9
1:1 Perfluoropentane: Perfluorohexane (C_5C_6)	Large	AF680 Dextran	3.4	0.1	20.8	0.4	1.5E + 10	2.2E + 8	2.1	0.1	72.7	5.1
	Small	AF680 Dextran	2.9	0.1	10.7	0.1	1.1E + 11	6.6E + 8	2.3	0.1	67.4	3.7
100% Perfluorohexane (C_6)	Large	AF680 Dextran	3.5	0.1	21.5	0.9	2.3E + 10	2.1E + 9	2.5	0.1	75.9	2.0
	Small	AF680 Dextran/DPBS	2.8	0.1	10.6	0.1	1.0E + 11	6.3E + 8	2.7	0.1	70.0	8.6